Diffraction of plane P waves around an alluvial valley in poroelastic half-space[*]

Zhongxian Liu　and　Jianwen Liang [♣]

Department of Civil Engineering, Tianjin University, Tianjin 300072, China

Abstract　　Diffraction of plane P waves around an alluvial valley of arbitrary shape in poroelastic half-space is investigated by using an indirect boundary integral equation method. Based on the Green's functions of line source in poroelastic half-space, the scattered waves are constructed using the fictitious wave sources close to the interface of the valley and the density of fictitious wave sources are determined by boundary conditions. The precision of the method is verified by the satisfaction extent of boundary conditions, and the comparison between the degenerated solutions and available results in single-phase case. Finally, the nature of diffraction of plane P waves around an alluvial valley in poroelastic half-space is investigated in detail through numerical examples.

Key words: diffraction; plane P waves; alluvial valley; poroelastic half-space; indirect boundary integration equation method

CLC number: P315.3[+]1　　　**Document code**: A

1 Introduction

It is well known that alluvial valleys may result in large amplification of ground motion during earthquakes. In the early 1970s, Trifunac (1971) developed an exact solution for diffraction of plane SH waves around a semi-cylindrical alluvial valley. Then many studies have been made on this topic. In these studies there are analytical solutions (e.g., Wong and Trifunac, 1974; Todorovska and Lee, 1991; Yuan and Liao, 1995) and numerical solutions (e.g., Boore et al, 1971; Kawase and Aki, 1989; Du et al, 1993; Sanchez-Sesma et al, 1993; Liao, 2002; Zhou and Chen, 2008). The analytical method is often referred to as wave function expansion method, and the numerical method includes finite difference method, finite element method, boundary element method, discrete wave number method, wave source method, etc.

It should be noted that soil media are often saturated in reality, especially in coastal region. Li et al (2005) and Zhou et al (2008) studied diffraction of elastic waves around a valley in poroelastic half-space using wave function expansion method and complex function

method, respectively. However, in these studies there exists an approximation to some extent by introducing a very big circular-arc to imitate the surface of half-space (Lee and Liang, 2008).

In recent years, a special indirect boundary integral equation method (IBIEM) has been applied to the field of diffraction of plane waves in elastic media (Wong, 1982; Dravinski and Mossessian, 1987; de Barros and Luco, 1995), and has been extended to the case of poroelastic media by Liang and Liu (2009a, 2009b). It is illustrated that this method has several advantages, such as reducing dimensions of problems, automatic satisfaction of radiation condition, and high calculation precision. Based on Green's function by Liang and Liu (2009b), this method is further extended to the solution for diffraction of elastic waves around alluvial valleys in poroelastic half-space. The nature of diffraction of plane P waves around an alluvial valley is investigated in detail through numerical examples, and some conclusions are obtained.

2 Formulation

2.1 Model

The problem to be studied is the 2-D diffraction of plane P waves around an alluvial valley of arbitrary shape in poroelastic half-space, as shown in Figure 1. Both the half-space (D_1) and the valley (D_2) are assumed

---

to be poroelastic, homogeneous and isotropic. The symbol S refers to the interface between the half-space and the valley. To construct the diffracted waves in the half-space and the valley, fictitious wave sources are introduced close to the interface S, forming two fictitious surfaces S_1 and S_2, inside and outside the valley, respectively.
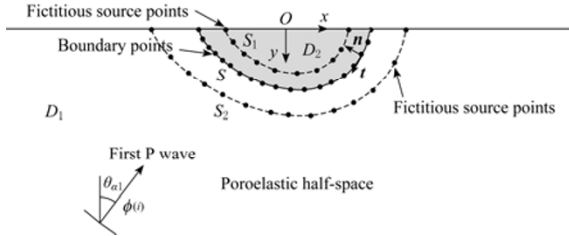

Figure 1 The model.

2.2 Biot's theory

If the displacement of the solid frame and the fluid displacement relative to the solid frame are denoted by u_i and w_i ($i=x, y$), respectively, the constitutive relations of a homogeneous poroelastic medium can be expressed as (Biot, 1941)

$$\sigma_{ij} = 2\mu\varepsilon_{ij} + \lambda\delta_{ij}e - \alpha\delta_{ij}p \qquad i,j=x,y, \quad (1)$$

$$p = -\alpha M u_{i,i} - M w_{i,i}, \quad (2)$$

in which, σ_{ij} is total stress component of the bulk material, ε_{ij} and e are strain components and dilatation of the solid frame, respectively; λ and μ are Lame constants of the bulk material, p is pore pressure, δ_{ij} is Kronecker delta, α and M are Biot's parameters describing compressibility of the two-phase material, and $0\leq\alpha\leq1$ and $0\leq M\leq\infty$.

The motion equations of a homogeneous poroelastic medium can be expressed in terms of displacements u_i and w_i as (Biot, 1962)

$$\mu u_{i,jj} + (\lambda + \alpha^2 M + \mu)u_{j,ji} + \alpha M w_{j,ji} = \rho\ddot{u}_i + \rho_{\rm f}\ddot{w}_i, \quad (3)$$

$$\alpha M u_{j,ji} + M w_{j,ji} = \rho_{\rm f}\ddot{u}_i + m\ddot{w}_i + b\dot{w}_i, \quad (4)$$

where $\rho=(1-n)\rho_{\rm s}+n\rho_{\rm f}$, $\rho_{\rm s}$ and $\rho_{\rm f}$ are mass density of the solid grain and the pore fluid, respectively, n is porosity of the solid frame; b is a parameter accounting for the internal friction due to the relative motion between the solid frame and the pore fluid, and $b=0$ if the internal friction is neglected; m is a density-like parameter depending on $\rho_{\rm f}$ and the geometry of the pores.

Based on Biot's theory, there exist two compressional (P) waves and one shear (S) wave in poroelastic

medium. Let $k_{\alpha1}$, $k_{\alpha2}$ and k_β denote the wave numbers for these waves, respectively, then for steady-state response, the two P wave potentials ϕ_1 and ϕ_2 and the S wave potential ψ for the solid frame satisfy the following equations:

$$\nabla^2\phi_1 + k_{\alpha1}^2\phi_1 = 0, \quad (5a)$$

$$\nabla^2\phi_2 + k_{\alpha2}^2\phi_2 = 0, \quad (5b)$$

and

$$\nabla^2\psi + k_\beta^2\psi = 0, \quad (5c)$$

where ∇^2 is the Laplace operator defined by

$$\nabla^2 = \frac{\partial}{\partial x^2} + \frac{\partial}{\partial y^2}.$$

To clarify the waves in D_1 and D_2, the wave numbers of two P waves and SV wave are represented by $k_{\alpha11}$, $k_{\alpha21}$ and $k_{\beta1}$ in half-space, respectively, and $k_{\alpha12}$, $k_{\alpha22}$ and $k_{\beta2}$ for the alluvial valley, correspondingly.

2.3 Wave fields
2.3.1 Free field

Consider a poroelastic half-space subjected to incident plane first P waves, the potentials of incident waves can be expressed by

$$\phi^{(\rm i)}(x,y) = \exp[-{\rm i}k_{\alpha11}(x\sin\theta_{\alpha1} - y\cos\theta_{\alpha1})], \quad (6)$$

where $\theta_{\alpha1}$ represents the incident angle. The time factor $\exp({\rm i}\omega t)$ is omitted here and thereafter. The first P wave incident on the surface of the poroelastic half-space will generate one reflected first P wave, one reflected second P wave and one reflected SV wave, which can be expressed as (Lin et al, 2005)

$$\phi_1^{(\rm r)}(x,y) = a_1\exp[-{\rm i}k_{\alpha11}(x\sin\theta_{\alpha1} + y\cos\theta_{\alpha1})], \quad (7)$$

$$\phi_2^{(\rm r)}(x,y) = a_2\exp[-{\rm i}k_{\alpha21}(x\sin\theta_{\alpha2} + y\cos\theta_{\alpha2})], \quad (8)$$

$$\psi^{(\rm r)}(x,y) = b\exp[-{\rm i}k_{\beta1}(x\sin\theta_\beta + y\cos\theta_\beta)], \quad (9)$$

where a_1, a_2 and b are reflection coefficients. The stress $\sigma_{ij}^{\rm f}$, solid frame displacement $u_i^{\rm f}$, fluid relative displacement $w_i^{\rm f}$, and pore pressure $p^{\rm f}$ of the free field can be obtained.

2.3.2 Diffracted waves

In the presence of the alluvial valley, diffracted waves are generated. In this paper, the diffracted waves inside and outside the alluvial valley are constructed by fictitious wave sources placed on the surfaces S_1 and S_2, respectively.

The displacements and stresses in the half-space due to the diffracted wave field can be expressed as

$$u_i^s(x) = \int_b [b(x_1)G_{i,1}^{(s)}(x,x_1) + c(x_1)G_{i,2}^{(s)}(x,x_1) + d(x_1)G_{i,3}^{(s)}(x,x_1)]dS_1, \quad (10)$$

$$\sigma_{ij}^s(x) = \int_b [b(x_1)T_{ij,1}^{(s)}(x,x_1) + c(x_1)T_{ij,2}^{(s)}(x,x_1) + d(x_1)T_{ij,2}^{(s)}(x,x_1)]dS_1, \quad (11)$$

$$w_i^s(x) = \int_b [b(x_1)G_{wi,1}^{(s)}(x,x_1) + c(x_1)G_{wi,2}^{(s)}(x,x_1) + d(x_1)G_{wi,3}^{(s)}(x,x_1)]dS_1, \quad (12)$$

$$p^s(x) = \int_b [b(x_1)T_{p,1}^{(s)}(x,x_1) + c(x_1)T_{p,2}^{(s)}(x,x_1) + d(x_1)T_{p,3}^{(s)}(x,x_1)]dS_1, \quad (13)$$

in which, $x \in D_1$, $x_1 \in S_1$; $b(x_1)$, $c(x_1)$ and $d(x_1)$ are the amplitudes for the two P waves and the SV wave at position x_1 in the fictitious surface S_1; $G_{i,l}^{(s)}(x,x_1)$, $G_{wi,l}^{(s)}(x,x_1)$, $T_{ij,l}^{(s)}(x,x_1)$ and $T_{p,l}^{(s)}(x,x_1)$ are the Green's functions for solid frame displacement, fluid relative displacement, stress and pore pressure in the half-space (subscript l=1, 2, 3 for first P wave, second P wave and SV wave sources, respectively). These Green's functions already satisfy the wave motion equation and the boundary condition of free surface. The expression of these Green's functions can be found in paper (Liang and Liu, 2009b).

Then the displacement field and stress field in the half-space can be obtained by

$$u_i(x) = u_i^f(x) + u_i^s(x), \quad (14a)$$

$$\sigma_{ij}(x) = \sigma_{ij}^f(x) + \sigma_{ij}^s(x), \quad (14b)$$

$$w_i(x) = w_i^f(x) + w_i^s(x), \quad (14c)$$

and

$$p(x) = p^f(x) + p^s(x). \quad (14d)$$

In the same way, the displacements and stresses in the alluvial valley can be expressed as

$$u_i(x) = \int_b [e(x_2)G_{i,1}^{(v)}(x,x_2) + f(x_2)G_{i,2}^{(v)}(x,x_2) + g(x_2)G_{i,3}^{(v)}(x,x_2)]dS_2, \quad (15)$$

$$\sigma_{ij}(x) = \int_b [e(x_2)T_{ij,1}^{(v)}(x,x_2) + f(x_2)T_{ij,2}^{(v)}(x,x_2) + g(x_2)T_{ij,2}^{(v)}(x,x_2)]dS_2, \quad (16)$$

$$w_i(x) = \int_b [e(x_2)G_{wi,1}^{(v)}(x,x_2) + f(x_2)G_{wi,2}^{(v)}(x,x_2) + g(x_2)G_{wi,3}^{(s)}(x,x_2)]dS_2, \quad (17)$$

$$p(x) = \int_b [e(x_2)T_{p,1}^{(v)}(x,x_2) + f(x_2)T_{p,2}^{(v)}(x,x_2) + g(x_2)T_{p,3}^{(v)}(x,x_2)]dS_2, \quad (18)$$

in which, $x \in D_2$, $x_2 \in S_2$; $e(x_2)$, $f(x_2)$ and $g(x_2)$ are the amplitudes for the two P waves and the SV wave at position x_2 in the fictitious surface S_2; $G_{i,l}^{(v)}(x,x_2)$, $G_{wi,l}^{(v)}(x,x_2)$, $T_{ij,l}^{(v)}(x,x_2)$ and $T_{p,l}^{(v)}(x,x_2)$ are the Green's functions for solid frame displacement, fluid relative displacement, stress and pore pressure in the alluvial valley.

2.4 Boundary condition

The boundary conditions of this problem include traction free conditions on the surface of the half-space, and the continuity conditions along the interface S. Because the boundary conditions at the surface of the valley and the half-space are satisfied already, only the continuity boundary conditions need to be considered.

The drained and undrained conditions at the interface are usually assumed for such problem (Figures 2a and 2c). However, the partially drained condition is more common in reality (Figure 2b). Based on the work of Deresiewicz (1963), the boundary conditions are defined as

$$u_x^s = u_x^v \quad u_y^s = u_y^v \quad w_n^s = w_n^v, \quad (19a)$$

$$\sigma_{nn}^s = \sigma_{nn}^v \quad \sigma_{nt}^s = \sigma_{nt}^v, \quad (19b)$$

$$p^s - p^v = k\dot{w}_n, \quad (19c)$$

where superscript "s" and "v" represent the half-place and the alluvial, respectively; the symbol k is a coefficient of resistance, which represents a measure of restriction of the flow across the interface resulting from imperfect alignment of the interfacial pores; $\dot{w}_n$ is the normal component of the relative velocity of liquid with respect to solid phase. For two limiting cases, equation (19c) can be reduced to

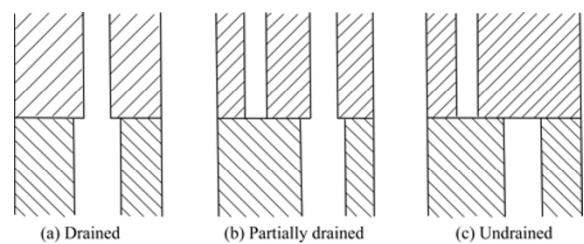$$p^s - p^v = 0 \quad k=0, \text{ drained case} \quad (20a)$$

or

Figure 2 Drainage conditions at the interface (Deresiewicz, 1963).

$$\dot{w}_n = 0 \quad k=\infty, \text{ undrained case.} \tag{20b}$$

To obtain the numerical solution, it is necessary to discretize the interface S and the wave source surfaces S_1 and S_2, which is shown in Figure 1. If the numbers of the discrete points on the surfaces S, S_1 and S_2 are N, N_1 and N_2 ($N{\geq}N_1$, $N{\geq}N_2$), respectively, the displacement and stress of the scattered field in the half-space can be written as

$$u_i^s(x_n) = b_{n1}G_{i,1}^{(s)}(x_n, x_{n1}) + c_{n1}G_{i,2}^{(s)}(x_n, x_{n1}) +$$
$$d_{n1}G_{i,3}^{(s)}(x_n, x_{n1}), \tag{21}$$

$$w_i^s(x_n) = b_{n1}G_{wi,1}^{(s)}(x_n, x_{n1}) + c_{n1}G_{wi,2}^{(s)}(x_n, x_{n1}) +$$
$$d_{n1}G_{wi,3}^{(s)}(x_n, x_{n1}), \tag{22}$$

$$\sigma_{ij}^s(x_n) = b_{n1}T_{ij,1}^{(s)}(x_n, x_{n1}) + c_{n1}T_{ij,2}^{(s)}(x_n, x_{n1}) +$$
$$d_{n1}T_{ij,3}^{(s)}(x_n, x_{n1}), \tag{23}$$

$$p^s(x_n) = b_{n1}T_{p,1}^{(s)}(x_n, x_{n1}) + c_{n1}T_{p,2}^{(s)}(x_n, x_{n1}) +$$
$$d_{n1}T_{p,3}^{(s)}(x_n, x_{n1}), \tag{24}$$

where $x_n{\in}S$, $x_{n1}{\in}S_1$; $n=1, 2, \cdots, N$; $n1=1, 2, \cdots, N_1$; b_{n1}, c_{n1} and d_{n1} are the densities of the first P wave, the second P wave and the SV wave at $n1$th source, respectively.

As for the wave field inside the alluvium, the surface S_2 can be discretized in the same way, and the densities of the first P wave, the second P wave and the SV wave at $n2$th source on S_2 can be denoted by e_{n2}, f_{n2} and g_{n2}.

Then from the boundary conditions (19), the following equations can be obtained:

$$\boldsymbol{H}_1\boldsymbol{Y}_1 + \boldsymbol{F} = \boldsymbol{H}_2\boldsymbol{Y}_2, \tag{25}$$

in which, $\boldsymbol{H}_1(6N, 3N_1)$, $\boldsymbol{H}_2(6N, 3N_2)$ are influence matrix which corresponds to the displacement and stress due to fictitious wave sources on the surface S_1, S_2, respectively. $\boldsymbol{Y}_1(3N_1, 1)$ and $\boldsymbol{Y}_2(3N_2, 1)$ are unknown density vector. $\boldsymbol{F}(6N, 1)$ is the displacement and stress vector of free field. The equation can be solved by using least-squares method. Once the unknown wave source density is calculated, the whole wave field can be obtained through superposition of diffracted field and free field.

3 Numerical implementation

Compared with other boundary integral equation methods, one prominent character of this method is that the singularity is avoided because the wave sources are located at the fictitious surface S_1 (close to but not on the valley boundary S). The numerical experiments show that at least seven discrete points per wave-length are required on the boundary. For incident frequency $\eta{\leq}2.0$ (η is the dimensionless frequency defined later) the number of the wave sources can approximately take 0.5–0.8 times the number of discrete points of valley boundary, and the wave sources should better be placed within 0.4–0.6 times of the relevant radii of the valley; however, for higher incident frequency $\eta>2.0$ the wave sources should be placed within 0.7–0.9 times of the relevant radii of the valley, and the number of the wave sources can approximately take 0.8–0.9 times of that of discrete points of valley boundary. For convenience, S_1 and S_2 follow the shape of S, and the distances between S_2 and S are identical to those between S_1 and S.

It is worth noting that the Green's functions of line source in poroelastic half-space are computed by Fourier transformation in space-wave number domain. To consider the material damping, linear complex hysteretic damping is introduced by $\bar{\lambda} = \lambda(1+2\zeta i)$ and $\bar{\mu} = \mu(1+2\zeta i)$, in which, ζ is the damping ratio. Then the seven-point Gaussian integration is used to compute the Green's function in this paper, in which, different integration intervals are used for different incident frequency to improve the computation efficiency. It should be noted that for $\eta=2$ ($N=41$, $N_1=25$), the computation can be completed within 10 minutes on a common personal computer with CPU 2.40 GHz and memory 2.0 Gb.

4 Accuracy verification

Accuracy of numerical results is verified for the case of a semi-circular alluvial valley. Because there is no exact solution for the diffraction of plane waves by an alluvial valley in poroelastic half-space up to now, the verification is performed by the check of satisfaction extent of boundary conditions and the comparison between the degenerated solutions of single-phase half-space and the well-known solutions.

The dimensionless incident frequency is defined as $\eta=\omega a/\pi c_\beta$, where a is radius of the valley, c_β is the shear wave velocity in half-space.

The check of boundary conditions shows that the stress residuals gradually decrease as the number of discrete points of the interface increases. Even for high incident frequency $\eta=3.0$, the normalized stress residual (normalized by the stress intensity of the incident P waves) can reach to a level of 10^{-3} for $N=81$ and $N_1=61$.

For the degenerated solution of single-phase

half-space, the following parameters associated with poroelasticity are taken: $M^*=\rho_f^*=m^*=\alpha=0$, and with the shear modular ratio $\mu^*=1/6$, the damping ratio $\zeta=0.001$, Poisson's ratio $\nu=1/3$ and incident frequency $\eta=1.0$. Figure 3 shows the surface displacement amplitudes of the half-space compared with the well-known results of single-phase half-space by Dravinski and Mossessian (1987) for incident angle $\theta_{\alpha 1}=0°$ and $\theta_{\alpha 1}=30°$, respectively. It is shown that the results in the present study are in excellent agreement with the results of Dravinski and Mossessian (1987).
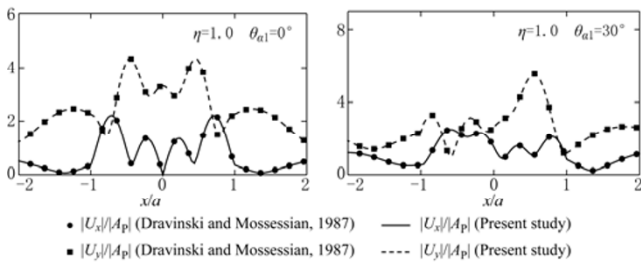
Figure 3 Degenerated frequency solution compared with the results of Dravinski and Mossessian (1987).

5 Numerical results and discussion

The parameters of saturated poroelastic media in the half-space are defined as follows: Poisson's ratio $\nu=0.25$, porosity $n_s=0.3$, the bulk modulus of the solid grain $K_{gs}=36$ GPa, the bulk modulus of fluid $K_f=2$ GPa, the mass density of the solid grain $\rho_s=2.65\times10^3$ kg/m^3, the mass density of fluid $\rho_f=1.0\times10^3$ kg/m^3. The corresponding parameters are taken: $\lambda^*=1.0$, $M^*=1.64$, $\rho^*=0.46$, $m^*=3.35$, $\alpha=0.28$. The material parameters of saturated poroelastic medium inside the valley are listed in Table 1 for different porosities ($\lambda^*=\lambda/\mu$, $M^*=M/\mu$, $\rho^*=\rho_f/\rho$, $m^*=m/\rho$). It should be noted that the bulk modulus of the solid grain $K_{gv}=9$ GPa, the critical bulk modulus of the solid frame $K_{cr}=50$ MPa, and the critical porosity $n_{cr}=0.36$. The linear hysteretic damping ratio $\zeta=0.001$ is used for the following study.

Figures 4 to 6 illustrate the horizontal ($|U_x|/|A_P|$) and vertical ($|U_y|/|A_P|$) surface displacement amplitudes near

Table 1 Properties of poroelastic medium inside the valley for different porosities

n_v	λ^*	M^*	ρ^*	m^*	α
0.30	1.00	5.18	0.46	3.35	0.83
0.34	1.00	12.87	0.48	2.77	0.94
0.36	1.00	133.1	0.49	2.55	0.99

Note: n_v is porosity, ρ_f is mass density of the pore fluid, λ and μ are Lame constants of the bulk material, ρ is density, M is a Biot's parameter describing compressibility of the two-phase material, and m is a density-like parameter depending on ρ_f and the geometry of the pores; $\lambda^*=\lambda/\mu$, $M^*=M/\mu$, $\rho^*=\rho_f/\rho$, $m^*=m/\rho$.

Figure 4 Surface displacement amplitudes of dry poroelastic, drained poroelastic, and undrained poroelastic half-spaces ($\eta=0.5$, $n_s=0.3$, $n_v=0.3$).
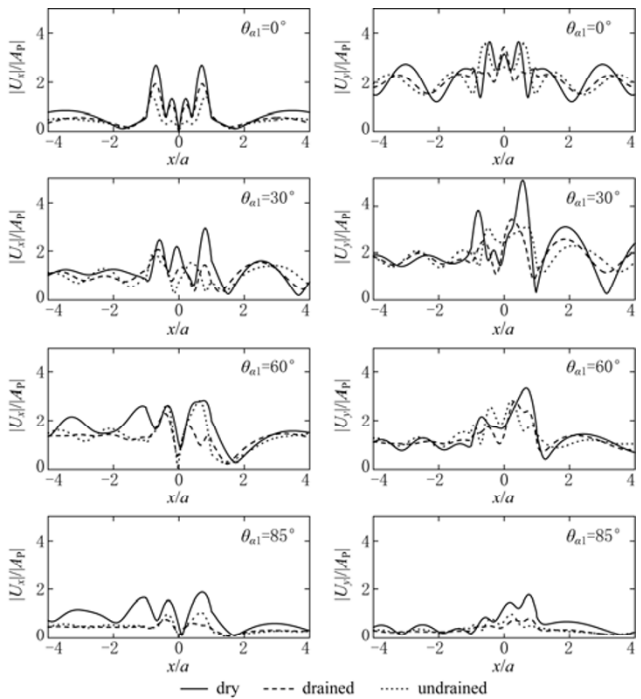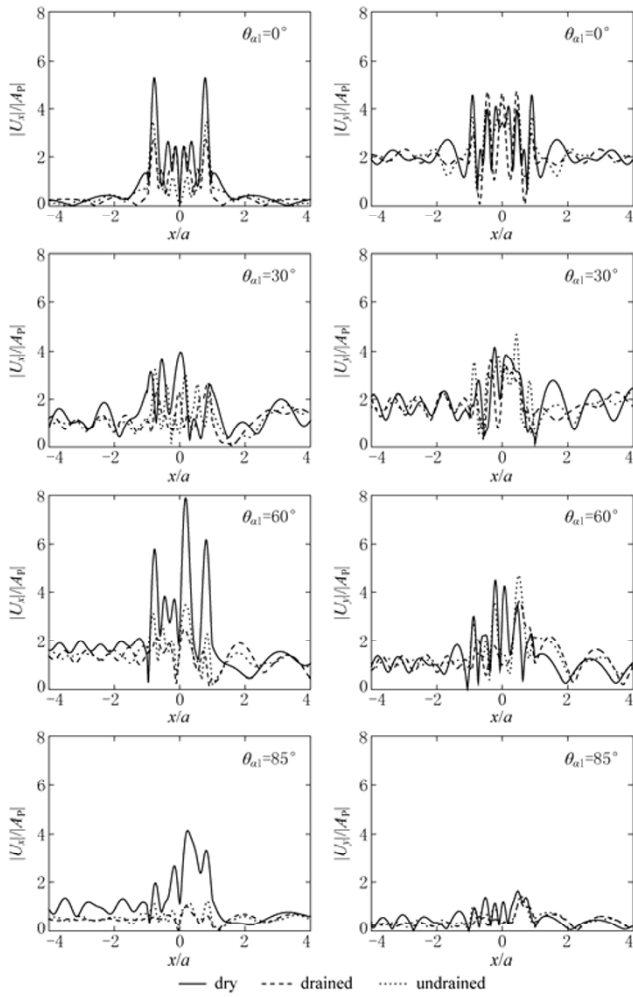
Figure 5 Surface displacement amplitudes of dry poroelastic, drained poroelastic, and undrained poroelastic half-spaces ($\eta=1.0$, $n_s=0.3$, $n_v=0.3$).

Figure 6 Surface displacement amplitudes of dry poroelastic, drained poroelastic, and undrained poroelastic half-spaces (η=2.0, n_s=0.3, n_v=0.3).

the valley in a dry poroelastic half-space, drained poroelastic half-space and undrained poroelastic half-space, respectively, for porosity n_s=0.3 and n_v=0.3, dimensionless incident frequency η=0.5, 1.0, and 2.0, and incident angle $\theta_{\alpha 1}$=0°, 30°, 60° and 85°, respectively. The surface displacement amplitudes are normalized by the displacement amplitude of the incident P wave. It is shown that the surface displacement amplitudes of the dry case are significantly different from those of the saturated (either drained or undrained) cases, and the drainage condition has large effect on the surface displacement amplitude; the displacement amplitudes of the dry case are usually larger than that of the undrained case, and the displacement amplitudes of the undrained case are usually larger than that of the drained case. From these figures phase shift can also be easily observed between the dry case and the saturated cases, as

well as the slightly longer resultant wavelengths for the undrained case than those for the drained case and the longer resultant wavelengths for the drained case than those for the dry case.

Figures 7 illustrates the horizontal and vertical surface displacement amplitudes near the valley under different drainage condition on interface S (the flat ground surface is assumed to be drained), for η=0.5, 1.0 and 2.0, and for k=0 (drained), 5, 10, 20, and ∞ (undrained), respectively, in which, the case $0 < k < \infty$ corresponds to the condition of partially drained. Other parameters are identical to the above examples. As shown in these figures, with the increase of the resistance coefficient, the displacement amplitudes gradually approach to that of the undrained case. From these results, it may be suggested that k=5 may be approximately defined as semi-drained condition in this study.
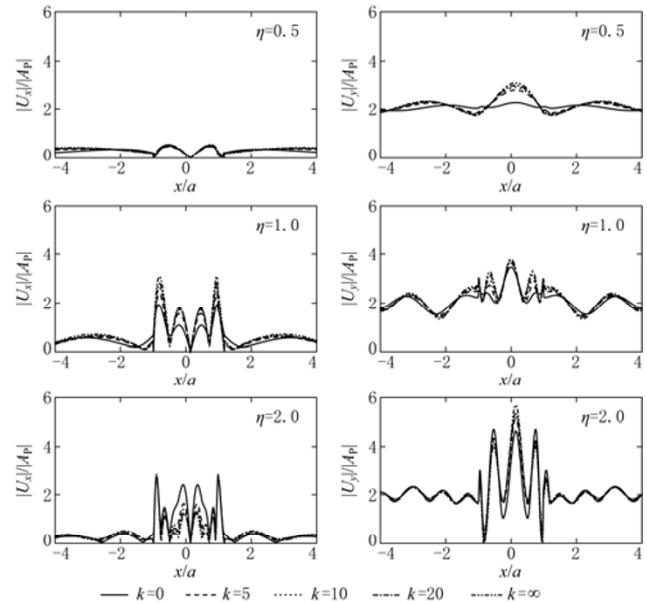

Figure 7 Surface displacement amplitude near the valley with variation of resistance coefficient k (n_s=0.3, n_v=0.3).

Figure 8 illustrates the surface pore pressures along the interface between the valley and the half-space (undrained conditions at the interface and the ground surface), for porosity n_s=0.3 and n_v=0.3, Poisson's ratio ν=0.25. The surface pore pressures are normalized by the stress intensity of the incident P wave. It can be seen from Figure 8 that large pore pressures occur along the interface, and the pore pressures depend strongly on the incident angle and the incident frequency. The pore pressures are smooth along the interface for the lower incident frequency and become more complicated with the

increase of the incident frequency, which suggests that the higher-frequency waves more easily stimulate pore pressures of large amplitudes and of rapid oscillations.

Figures 9 to 11 and Figures 12 to 14 illustrate the normalized horizontal and vertical displacement amplitudes around the valley, for drained and undrained boundary conditions, respectively. The parameters are defined as follows: porosity $n_s=0.3$ and $n_v=0.3$, 0.34 and 0.36, Poisson's ratio $\nu=0.25$, dimensionless incident frequency $\eta=0.5$, 1.0 and 2.0, and incident angle $\theta_{\alpha 1}=0°$, 30°, 60° and 85°, respectively. It can be seen from these figures that the porosity of the valley has significant effect on the surface displacement amplitudes both for the drained and undrained cases. As the increase of the
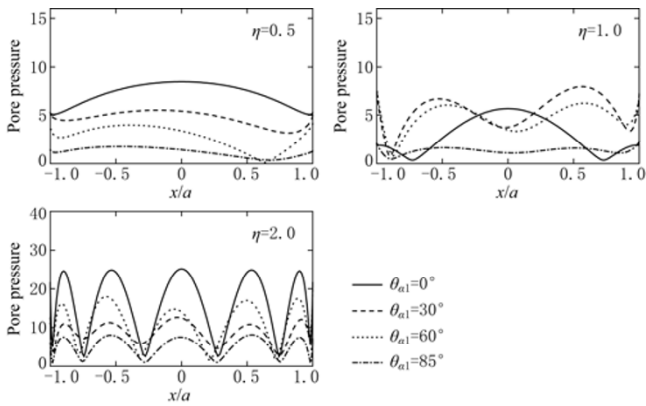

Figure 8 Pore pressure around the interface under different incident angles for undrained boundary ($n_s=0.3$, $n_v=0.3$).
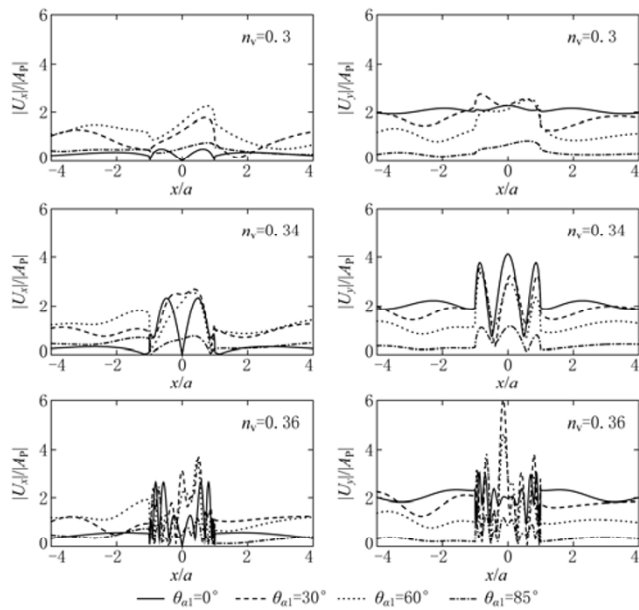

Figure 9 Surface displacement amplitude for different porosities for drained boundary ($\eta=0.5$, $n_s=0.3$).
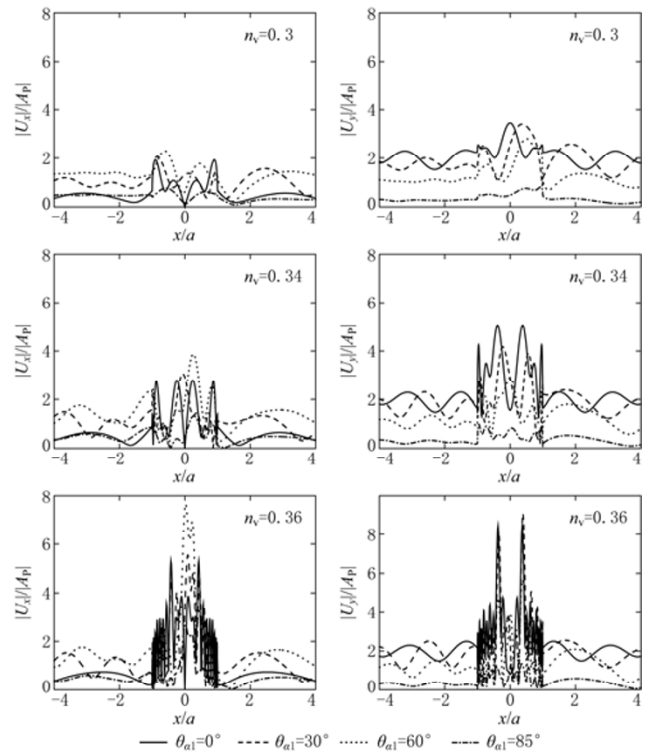

Figure 10 Surface displacement amplitude for different porosities for drained boundary ($\eta=1.0$, $n_s=0.3$).
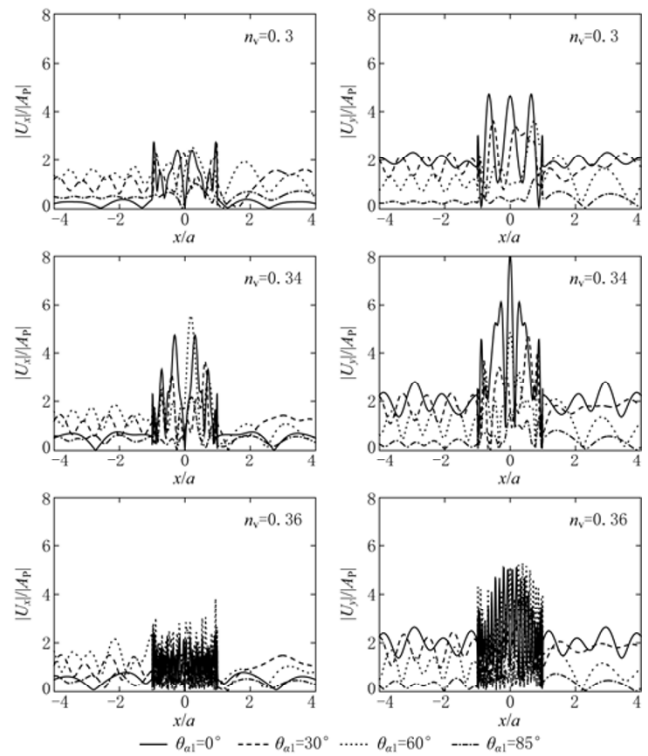

Figure 11 Surface displacement amplitude for different porosities for drained boundary ($\eta=2.0$, $n_s=0.3$).
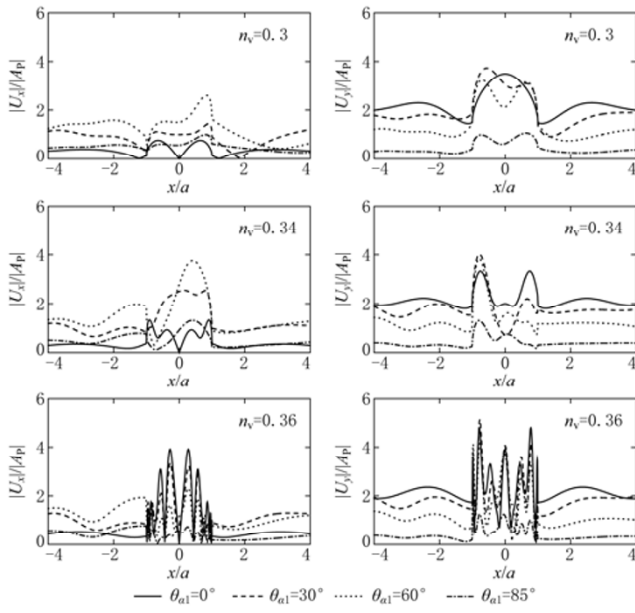
Figure 12   Surface displacement amplitude for different porosities for undrained boundary (η=0.5, n_s=0.3).

porosity of the valley, the surface displacement amplitudes increase and the surface displacement amplitude gradually become complicated with rapid oscillation, especially for the case of critical porosity and for higher
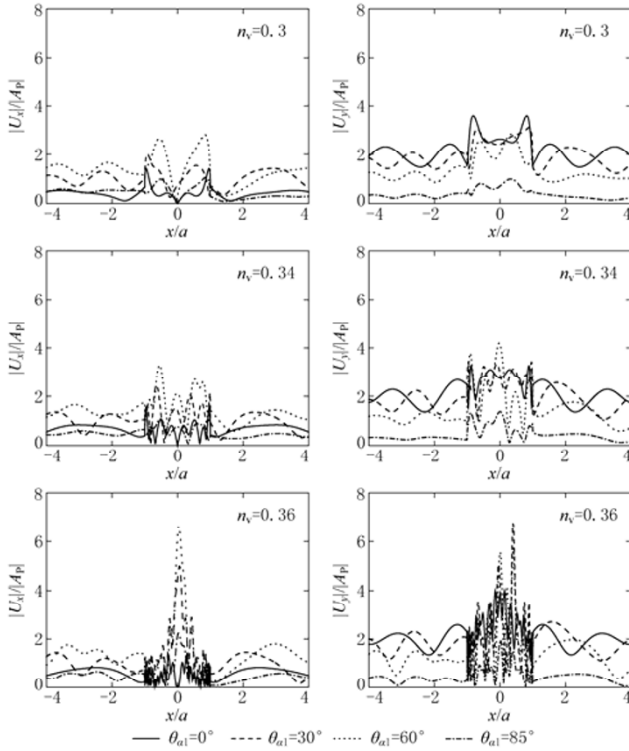
incident frequency.

6 Conclusions

Based on the Green's functions of line source in poroelastic half-space, the diffraction of plane P waves around an alluvial valley is solved by the indirect boundary integration equation method in this paper. The nature of diffraction of plane P waves around an alluvial valley was investigated, and the effects of drainage condition, porosity, incident frequency and incident angle on the diffraction of waves were studied in detail. Some conclusions are obtained.

Surface displacement amplitudes of the dry case are significantly different from those of the saturated (either drained or undrained) cases, and the drainage condition has large effect on the surface displacement amplitude; the displacement amplitudes of the dry case are usually larger than that of the undrained case, and the displacement amplitudes of the undrained case are usually larger than that of the drained case. Phase shift can be easily observed between the dry case and the saturated cases, as well as the slightly longer resultant wavelengths for the undrained case than those for the drained case and the longer resultant wavelengths for
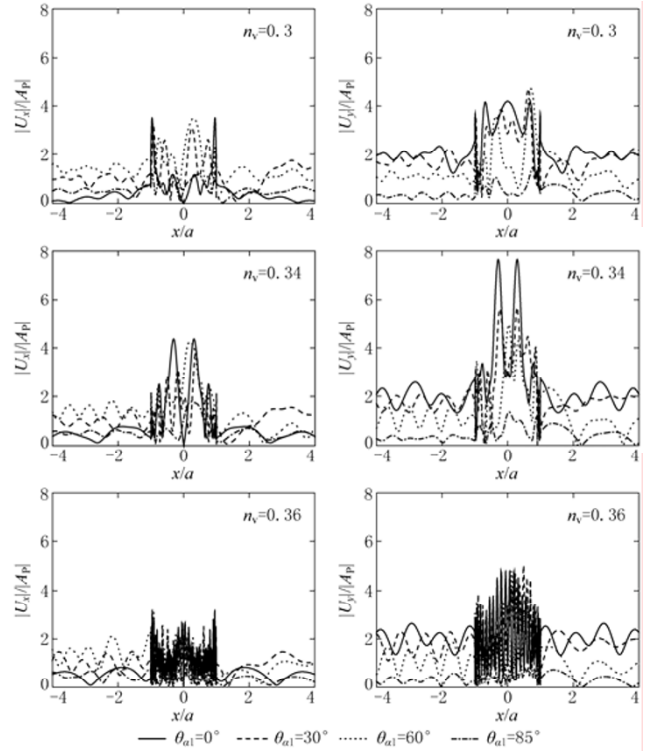

Figure 13   Surface displacement amplitude for different porosities for undrained boundary (η=1.0, n_s=0.3).

Figure 14   Surface displacement amplitude for different porosities for undrained boundary (η=2.0, n_s=0.3).

the drained case than those for the dry case. Porosity of the valley has significant effect on the surface displacement amplitudes both for the drained and undrained cases. As the increase of the porosity of the valley, the surface displacement amplitudes increase and the surface displacement amplitude gradually become complicated with rapid oscillation.

It should be noted that the numerical examples are implemented for a semi-circular alluvial valley. However, this method can be used for alluvial valley of arbitrary shape. Moreover, it is convenient for this method to be used for the case of layered half-space with the corresponding dynamic Green's function.

References

Biot M A (1941). General theory of three-dimensional consolidation. *J Appl Phys* **12**(2): 155−164.

Biot M A (1962). Mechanics of deformation and acoustic propagation in porous media. *J Appl Phys* **33**(4): 1 482−1 498.

Boore D M, Larner K L and Aki K (1971). Comparison of two independent methods for the solution of wave scattering problems: response of a sedimentary basin to incident SH waves. *J Geophys Res* **76**: 558−569.

de Barros F C P and Luco J E (1995). Amplification of obliquely incident waves by a cylindrical valley embedded in a layered half-space. *Soil Dynam Earthq Eng* **14**(3): 163−175.

Deresiewicz H (1963). On uniqueness in dynamic poroelasticity. *Bull Seism Soc Amer* **53**: 595−626.

Dravinski M and Mossessian T K (1987). Scattering of plane harmonic P, SV, and Rayleigh waves by dipping layers of arbitrary shape. *Bull Seism Soc Amer* **77**: 212−235.

Du X L, Xiong J G and Guan H M (1993). Boundary integration equation method to scattering of plane SH waves. *Acta Seismologica Sinica* **6**(3): 609−618.

Kawase H and Aki K (1989). A study on the response of a soft basin for incident P, S, Rayleigh waves with special reference to the long duration observed in Mexico city. *Bull Seism Soc Amer* **78**: 1 361−1 382.

Lee V W and Liang J (2008). Free-field (elastic or poroelastic) half-space zero-stress or related boundary conditions. *Proceedings of* 14*th World Conference on Earthquake Engineering*. Beijing, October 12−17, Paper 03-03-0002.

Li W H, Zhao C G and Shi P X (2005). Scattering of plane P waves by circular-arc alluvial valleys with saturated soil deposits. *Soil Dynam Earthq Eng* **25**: 997−1 014.

Liang J and Liu Z (2009a). Diffraction of plane P waves by a canyon of arbitrary shape in poroelastic half-space (I): Formulation. *Earthquake Science* **22**(3): 215−222.

Liang J and Liu Z (2009b). Diffraction of plane SV waves by a cavity in poroelastic half-space. *Earthq Eng Eng Vib* **8**(1): 29−46.

Liao Z P (2002). *Introduction to Wave Motion Theories in Engineering*. Science Press, Beijing, 236−270 (in Chinese).

Lin C H, Lee V W and Trifunac M D (2005). The reflection of plane waves in a poroelastic half-space fluid saturated with inviscid fluid. *Soil Dynam Earthq Eng* **25**: 205−223.

Sanchez-Sesma F J, Ramos-Martinez J and Campillo M (1993). An indirect boundary element method applied to simulate the seismic response of alluvial valleys for incident P, S and Rayleigh waves. *Earthq Eng Struct Dynam* **22**: 279−295.

Todorovska M and Lee V W (1991). Surface motion of shallow circular alluvial valleys for incident plane SH waves: Analytical solution. *Soil Dynam Earthq Eng* **10**: 192−200.

Trifunac M D (1971). Surface motion of a semi-cylindrical alluvial valley for incident plane SH waves. *Bull Seism Soc Amer* **61**: 1 755−1 770.

Wong H L (1982). Effect of surface topography on the diffraction of P, SV, and Rayleigh waves. *Bull Seism Soc Amer* **72**: 1 167−1 183.

Wong H L and Trifunac M D (1974). Surface motion of a semi-elliptical alluvial valley for incident plane SH waves. *Bull Seism Soc Amer* **64**: 1 389−1 408.

Yuan X M and Liao Z P (1995). Scattering of plane SH waves by a cylindrical alluvial valley of circular-arc cross-section. *Earthq Eng Struct Dynam* **24**: 1 303−1 313.

Zhou H and Chen X F (2008). The localized boundary integral equation-discrete wave number method for simulating P-SV wave scattering by an irregular topography. *Bull Seism Soc Amer* **98**(1): 265−279.

Zhou X L, Jiang L F and Wang J H (2008). Scattering of plane wave by circular-arc alluvial valley in a poroelastic half-space. *J Sound Vib* **318**(4-5): 1 024−1 049.